THE ASTRONOMICAL JOURNAL VOLUME 106, NUMBER 4 OCTOBER 1993

THE INTERMEDIATE AGE OPEN CLUSTER NGC 7044

A. APARICIO
Instituto de Astrofísica de Canarias, E38200, La Laguna, Tenerife, Canary Islands, Spain
Electronic mail: aaj@iac.es

E. J. ALFARO[1]
Instituto de Astrofísica de Andalucía, Apartado 2144, E18080 Granada, Spain and Boston University, 725 Commonwealth Avenue, Boston, Massachusetts 02215
Electronic mail: alfaro@iaa.es

A. J. DELGADO[1]
Instituto de Astrofísica de Andalucía, Apartado 2144, E18080 Granada, Spain
Electronic mail: delgado@iaa.es

J. A. RODRÍGUEZ-ULLOA
Royal Greenwich Observatory-Observatorio del Roque de los Muchachos, Apartado 321, E38780, Santa Cruz de la Palma, Canary Islands, Spain and European Southern Observatory, Karl-Schwarzschildstrasse 2, D8046, Garching bei München, Germany
Electronic mail: jrodrigu@eso.org

J. CABRERA-CAÑO[1]
Instituto de Astrofísica de Andalucía, Apartado 2144, E18080 Granada, Spain
Electronic mail: cabrera@iaa.es

Received 1993 January 8; revised 1993 June 17

ABSTRACT

We present the photometric analysis for the open cluster NGC 7044, based on Johnson–Cousins $UBVR$ CCD observations of 896 stars in a region of $4'20'' \times 2'40''$ in the cluster field. Reddening and metallicity are estimated by means of the location of selected samples of members in the $(U-B)$ vs $(B-V)$ diagram, with respect to the lines of the Hyades ZAMS and giants. This selection is performed by considering the location of the representative points in both the V vs $(B-V)$ and V vs $(U-B)$ diagrams simultaneously. The final estimates are found to be very dependent on whether, and to what extent, reddening slopes and absorption coefficients are considered to vary with spectral type. Global considerations, based on the photometric information together with the results of the comparison with theoretical model isochrones, lead to the following set of values: $E(B-V)=0.57$, $[Fe/H]=0.0$, $(m-M)_0=12.4$, and $\log \mathrm{age}(y)=9.4$. We discuss to some extent the influence that varying absorption coefficients, published in the literature, would have on these estimates. Our color–magnitude (CM) diagram is compared with selected sets of isochrones, based on evolutionary models computed with and without considering convective overshooting from the stellar core during the phases of H and He core burning. Better general agreement is found when using the overshooting models, between predicted and observed features of the CM diagram, particularly in what concerns the properties of the so-called Red Giant Clump (RGC). With the adopted solution, NGC 7044 turns out to be one of the oldest intermediate-age clusters, very close to, or even beyond the limiting age separating the regimes of He flash and quiet onset of He burning in the red giant phase. The location of the RGC in absolute magnitude, together with the resulting $(B-V)_0$ at the turnoff, leads us to suggest that the efficiency of convective core overshooting in stars of masses around and below 1.5 $\mathscr{M}_\odot$ should be slightly higher than that of the models used. An analysis of the spatial distribution of the stars suggest that a mass segregation mechanism is acting in the cluster, in the sense that the most massive members are concentrated in the center. Luminosity and mass functions have been computed; a classical power law fitted to the latter results in a slope of $x=-1.66\pm0.06$.

1. INTRODUCTION

Rich open clusters are key objects for clarifying questions of galactic structure as well as for checking the details of stellar evolution models. In particular, old and intermediate-age open clusters play an important role in linking the theories of stellar and galactic evolution.

In this framework, of special relevance is a group of open clusters in the direction of the galactic anticenter whose study could bring new insights about the chemical evolution of the Milky Way (Janes 1988; Sandage 1988). As stressed many times (see, e.g., Gilmore 1990), esti-

[1]Visiting Astronomer, German-Spanish Astronomical Center, Calar Alto, operated by the Max Planck Institute fur Astronomie, Heidelberg, jointly with the Spanish Comisión Nacional de Astronomía.

 0004-6256/93/106(4)/1547/14/$0.90

mates of the radial composition gradient in the galactic disk, and of the age–metallicity relationship, are fundamental for testing models of galactic evolution. Two recent papers (Friel & Janes 1993; Geisler *et al.* 1992) have fueled the interest for new and independent determinations of physical parameters of clusters located close to the solar galactocentric radius. In this galactic region, some objects display a departure, towards lower values of metallicity, from the mean [Fe/H]-radius loci, stressing the previous impression regardering the existence of local metallicity variations in the disk (Geisler 1987; Boesgaard & Friel 1990).

In addition, intermediate-age open clusters are in an evolutive stage which is well suited to check the issue of convective overshooting (Barbaro & Pigatto 1984, hereafter referred to as B84; Bertelli *et al.* 1985; Mazzei & Pigatto 1988). These clusters have the turnoff mass near the critical value separating the domain of the core He flash from that of the mild He ignition. From a theoretical point of view, the predicted critical mass m_c is very dependent on whether or not overshooting from the convective stellar cores is considered in the model computation. Furthermore, we are constrained to this range of age to analyze the overshooting phenomenon on the basis of color–magnitude (CM) diagram morphological features, and the luminosity function of red giant stars. In older clusters, masses of stars at the turnoff are too small to contain convective cores, whereas in younger clusters with more massive stars, there are typically few, if any, red giants.

In this paper we present the Johnson–Cousins $UBVR$ CCD photometry of the rich, intermediate-age open cluster NGC 7044 ($\alpha=21^{\rm h}12^{\rm m}50^{\rm s}$, $\delta=42°32'$, $l=86.°4$, $b=-4.°2$; Equinox 1950). Its diameter, estimated on the plates of the Palomar Sky Survey, is about 5′. The only photometric study of this cluster up to date, was performed by Kałużny (1989), who obtained BV photometry for 1097 stars in the area of the cluster. Estimates for reddening, distance modulus, and age were calculated for NGC 7044 assuming solar abundance, and the location of the red giant clump (RGC), on the $M_V-(B-V)_0$ plane, to be similar to that of the clusters NGC 7789 and Praesepe. Obtaining high quality photometric measurements for the U band allows us to determine the reddening and metallicity in an independent manner and, hence, to recalculate the distance and age of NGC 7044. The paper has been divided into seven sections: in Sec. 2 we describe the observations and discuss the data reduction procedure; Sec. 3 deals with the photometric errors and the effects of crowding on the completeness of the sample; the description and analysis of the main features appearing in the photometric diagrams are reported in Sec. 4; the physical parameters of the cluster are discussed in Sec. 5; Sec. 6 deals with the properties of the Red Giant Clump; Sec. 7 contains comments on the spatial distribution of the stars in the cluster, and on the possible existence of mass segregation; Sec. 8 is devoted to the obtaining and discussion of the luminosity and mass functions; finally, Sec. 9 summarizes the main results and conclusions of our work.

TABLE 1. Journal of observations.

Date	Time (UT)	Filter	Exp. time (s)	FWHM (")
Aug.01.1989	02^h50^m	U	3600	1.0
Aug.02.1989	23^h40^m	B	1200	1.1
Aug.02.1989	23^h55^m	V	800	1.0
Aug.03.1989	00^h15^m	V	400	1.3
Aug.03.1989	00^h28^m	R	50	1.5
Aug.03.1989	01^h50^m	U	3600	1.6

2. OBSERVATIONS AND DATA REDUCTION

We have observed the stellar content of NGC 7044 using a 640×1024 pixels, thin, uncoated, RCA CCD detector at the prime focus of the 3.5 m telescope at Calar Alto (Spain). The pixel size is 15 μm or, equivalently, 0.″254. The frames were taken in 1989 August, under photometric conditions. Table 1 shows the journal of observations for the cluster data, including in the last column the stellar full width at half of maximum (FWHM) measured on each frame. FIGARO, DAOPHOT, and ALLSTAR (see Stetson 1987, for the two last) have been used on the VAX cluster of the Instituto de Astrofísica de Canarias and of the Isaac Newton Group, Observatorio del Roque de los Muchachos (Spain), to produce the photometry of the stars.

The instrumental magnitudes $m_{\rm ap}$ to be transformed to the standard photometric system are defined as $-2.5 \log N + C$, where N is the total number of photons detected by the CCD from a given star. The $m_{\rm ap}$ magnitudes can be best obtained in uncrowded frames through synthetic-aperture photometry, simply by summing up the CCD counts inside a circle of a given radius centered on the star, and subtracting the sky counts determined from an external concentric annulus. When crowding is relevant, as is the case of the frames of NGC 7044, PSF-fitting of each star profile by means of DAOPHOT+ALLSTAR or any other similar program becomes necessary, but the resulting PSF magnitudes $m_{\rm als}$ are affected by a zero-point departure, which is different from frame to frame. This is because the DAOPHOT+ALLSTAR fitting procedure only uses the central part of the stars (see Stetson 1987 for a thorough discussion of this issue). To determine this zero point, a number of isolated *good* stars were selected in each frame. All the detected stars, except the selected ones, were then subtracted from the frame, and synthetic-aperture photometry was performed for the selected stars on the subtracted frame. The magnitudes obtained like this are already the $m_{\rm ap}$ ones. The zero point of the ALLSTAR scale of magnitude was then determined for each frame, using weighted means. We obtained typical errors for the zero-point estimates of 0.020 mag in U, 0.013 in B, 0.008 in V, and 0.016 in R.

Subsequently, atmospheric extinction corrections for each night, and instrumental $m_{\rm ap}$ to Johnson–Cousins system transformation equations for the whole campaign were determined. To this purpose 57 measurements for a total of 15 standard stars from the lists of Landolt (1983) and Neckel & Chini (1980) were taken at each band during the four nights of the observing run. The intervals covered in magnitude and color indices with the standard sample, amount to $8.86 < V < 11.17$, $-0.58 < (U-B) < 1.78$, $-0.33 < (B-V) < 1.69$, and $-0.02 < (V-R) < 0.98$. Synthetic-aperture photometry for these stars was performed using the same aperture and sky annulus sizes as in the $m_{\rm als}$ to $m_{\rm ap}$ transformations. After correcting for atmospheric extinction, we arrive at the following set of equations, transforming into the Johnson–Cousins standard system:

$$V = v + 24.717 - 0.062(B-V), \quad (1)$$

$$(U-B) = -2.779 + 1.094(u-b), \quad (3)$$

$$(B-V) = -0.245 + 1.102(b-v), \quad (2)$$

$$(V-R) = -0.156 + 1.241(v-r), \quad (4)$$

where capital letters are the Johnson–Cousins magnitudes, and small letters are the instrumental $m_{\rm ap}$ ones. Figures 1(a) to 1(d) show, respectively, the residuals versus the corresponding color indices for each equation. The zero-point errors affecting this transformation are 0.026 mag in V, 0.022 in $(U-B)$, 0.011 in $(B-V)$, and 0.012 in $(V-R)$, which, added quadratically to the zero-point errors of the $m_{\rm als}$ to $m_{\rm ap}$ transformation, result in the following total errors: 0.03 in V, 0.02 in $(B-V)$, 0.03 in $(U-B)$, and 0.02 in $(V-R)$.

Photometry in V and in at least one more band has been obtained for 896 stars in the field of NGC 7044. The results are listed in a table (Table 2)[2] available on the ApJ-AJ CDROM series. The table contains an identification number (column 1), X and Y coordinates in pixels (columns 2 and 3), V magnitudes, and $(U-B)$, $(B-V)$, and $(V-R)$ color indices (columns 4 to 7). The finding chart of the measured stars is given in Fig. 2, representing an area of $4'20'' \times 2'40''$. In this figure the size of the circles is related to the brightness in V of the star, and the coordinates are CCD pixels as listed in the table.

3. PHOTOMETRIC ERRORS AND COMPLETENESS

The errors affecting the photometry of stars in a crowded field have been discussed by many authors (see, for example, Mateo & Hodge 1986; Stetson 1987; Chiosi *et al.* 1989; Aparicio *et al.* 1990; Vallenari *et al.* 1993). In a first approximation, the photometric errors would be related to the signal-to-noise ratio. The errors given by ALLSTAR are calculated as the mean square root of the residuals of the fitting of the PSF to the profile of the central part of each star. It is well known, however, that crowding is another important source of error in the photometry of a stellar field and that it may have large effects (likely to be the dominant ones) both on the resulting magnitudes and on the photometric completeness of the stellar sample. The usual technique, based on the injection of artificial

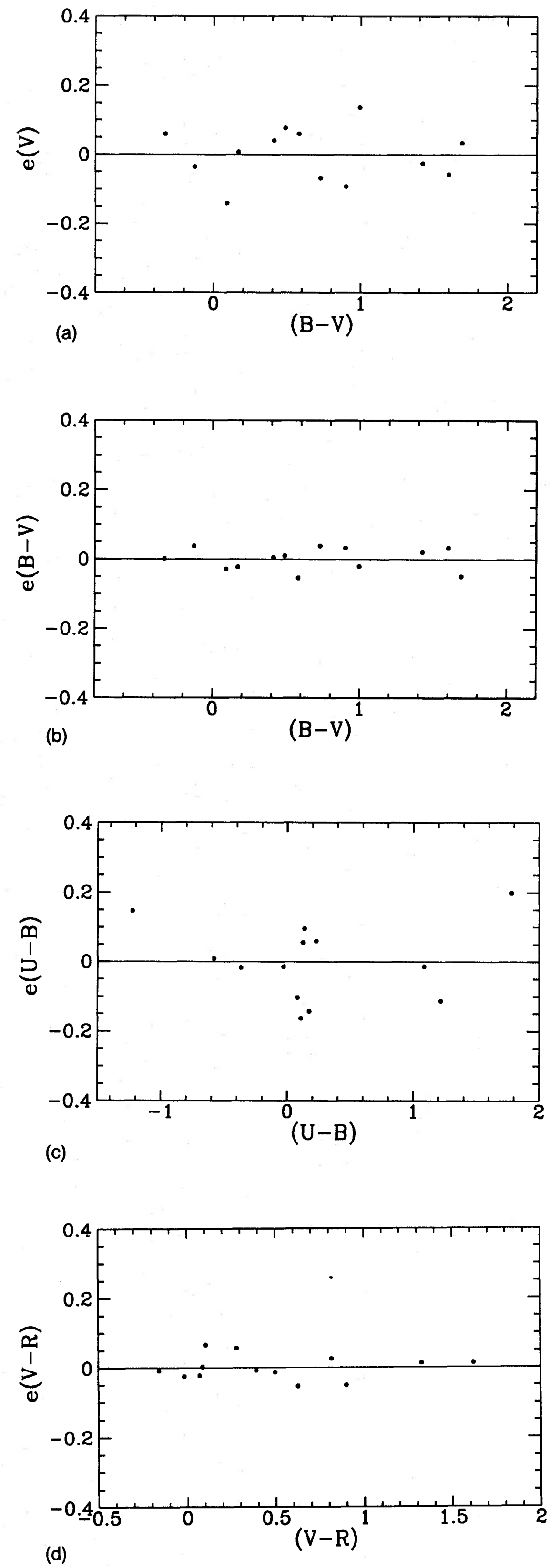

FIG. 1. (a)–(d). The residuals vs $(B-V)$, $(U-B)$, and $(V-R)$ color indices for the transformation from the instrumental to the Johnson–Cousins photometrical system.

[2]Table 2 is presented in its complete form in the ApJ/AJ CD-ROM Series, volume 1, 1993. The first page of this table is presented here for guidance regarding its form and content.

TABLE 2. Photometrical data of NGC 7044.

N	X	Y	V	(U−B)	(B−V)	(V−R)	N	X	Y	V	(U−B)	(B−V)	(V−R)
1	2.0	673.1	16.90	0.47	1.09	—	81	61.8	666.2	21.82	···	1.74	···
2	3.2	269.8	21.05	—	1.53	1.38	82	62.2	368.2	20.31	1.38	1.48	1.23
3	3.8	728.1	21.64	—	1.64	1.37	83	62.6	256.9	18.83	0.49	1.16	1.09
4	4.0	742.9	20.20	1.44	1.44	1.24	84	64.0	639.7	21.97	—	1.70	1.50
5	4.8	19.6	19.89	0.41	1.16	1.02	85	65.4	562.5	17.41	0.41	1.05	0.90
6	4.8	144.0	18.09	0.40	1.10	0.94	86	65.4	287.9	17.00	0.38	1.01	0.86
7	8.2	663.9	19.31	0.74	1.35	1.16	87	65.8	385.9	19.73	0.77	1.27	1.07
8	8.6	627.7	20.88	0.94	1.54	1.09	88	65.9	449.1	22.06	—	1.57	1.55
9	8.9	639.5	22.25	—	1.28	—	89	70.6	684.5	16.88	1.61	1.68	1.34
10	9.1	760.8	21.38	—	—	1.29	90	71.3	172.5	20.30	0.41	1.18	0.99
11	10.8	843.0	21.49	0.53	1.75	1.43	91	72.5	138.4	18.98	1.45	1.50	1.37
12	11.1	450.4	20.21	0.54	1.25	1.24	92	73.7	611.5	21.87	—	1.85	—
13	12.5	595.1	19.09	0.95	1.26	1.02	93	75.2	746.6	20.56	0.54	1.32	1.17
14	13.3	700.5	18.78	0.63	1.30	1.12	94	75.8	1016.3	20.61	—	1.52	1.24
15	14.0	100.1	18.03	0.41	1.12	0.98	95	76.4	204.3	16.72	0.47	1.03	0.87
16	14.5	810.0	22.44	—	1.14	1.18	96	76.4	466.3	21.73	—	1.16	1.01
17	14.6	58.4	20.01	0.91	1.31	1.08	97	76.9	949.8	19.29	0.66	1.27	1.08
18	15.3	654.2	18.06	0.49	1.14	0.98	98	78.3	422.8	18.76	0.47	1.15	1.00
19	15.5	365.7	19.92	1.46	1.67	1.35	99	78.4	721.8	21.10	0.73	1.36	1.19
20	15.7	288.9	17.46	0.41	1.08	0.92	100	78.8	934.8	21.96	—	1.46	1.33
21	16.8	376.3	20.80	1.07	1.44	1.18	101	79.0	87.5	22.23	—	1.68	1.56
22	16.8	647.0	20.44	—	1.36	··	102	79.3	319.0	22.42	—	1.61	1.40
23	17.1	894.3	20.95	—	1.63	1.49	103	80.8	365.3	21.01	—	1.50	1.33
24	17.4	388.1	17.99	0.59	1.08	0.89	104	81.1	220.1	21.67	0.34	1.38	—
25	18.0	418.2	22.57	—	1.60	1.91	105	82.1	187.7	18.77	0.50	1.16	1.01
26	18.0	195.7	18.09	0.40	1.08	0.92	106	82.4	418.2	19.92	0.61	1.24	1.05
27	18.0	406.9	20.66	1.20	1.41	1.20	107	82.8	905.7	21.56	0.74	1.54	1.24
28	18.3	790.3	19.04	0.73	1.35	1.12	108	83.6	331.7	22.73	—	1.36	—
29	18.3	45.4	21.80	—	1.79	1.41	109	83.7	538.8	19.65	0.74	1.20	1.07
30	19.0	520.2	21.27	—	1.47	1.27	110	83.8	737.9	16.69	0.55	1.15	0.96
31	20.5	931.4	21.02	0.70	1.32	1.23	111	84.0	20.2	15.10	—	—	1.50
32	20.7	185.3	19.41	0.60	1.23	1.03	112	84.2	649.3	19.31	0.62	1.25	1.06
33	21.7	105.9	21.93	—	1.53	—	113	85.5	230.6	19.35	0.55	1.22	1.07
34	21.7	667.7	21.55	—	—	1.32	114	87.7	620.8	22.11	—	1.42	1.17
35	22.0	498.8	18.38	0.43	1.10	0.92	115	88.3	406.0	20.77	—	1.52	1.30
36	22.5	152.4	16.44	0.47	1.13	0.95	116	88.4	509.3	18.66	0.49	1.13	0.97
37	22.7	299.1	21.95	—	1.76	1.35	117	88.6	680.7	14.83	1.91	1.75	1.38
38	24.4	541.4	17.39	0.43	1.06	0.90	118	89.1	776.6	19.19	0.72	1.31	1.10
39	24.5	688.5	18.88	0.52	1.25	1.04	119	90.3	273.0	15.70	1.40	1.56	1.22
40	25.4	623.0	21.78	—	1.47	0.94	120	91.2	752.9	21.55	—	1.79	1.50
41	25.9	717.9	20.10	0.85	1.46	1.23	121	91.5	804.8	21.18	—	1.71	1.64
42	26.3	8.3	16.71	0.43	1.06	0.89	122	92.0	948.0	20.45	—	1.45	1.28
43	27.9	560.2	17.58	0.41	1.05	0.89	123	93.6	862.0	22.81	—	2.00	1.92
44	28.9	644.5	16.97	0.33	1.00	0.85	124	93.6	101.2	19.46	0.44	1.14	1.00
45	29.3	937.2	20.93	0.42	1.32	0.87	125	93.8	455.8	21.07	0.63	1.35	1.06
46	30.4	167.0	19.80	—	—	1.45	126	95.0	847.4	19.42	0.62	1.29	1.05
47	30.7	57.8	20.27	0.52	1.23	1.06	127	95.3	666.9	20.36	1.28	1.64	1.28
48	33.7	630.7	21.90	—	1.03	1.22	128	96.5	349.8	18.28	0.43	1.00	0.94
49	35.8	723.3	19.02	0.61	1.29	1.11	129	96.1	225.7	20.98	—	1.54	1.21
50	36.0	120.8	22.29	—	1.85	—	130	97.2	971.7	19.13	1.34	1.39	1.18
51	37.8	301.3	19.66	0.96	1.35	1.16	131	98.1	544.1	20.27	0.83	1.41	1.09
52	38.0	480.7	18.14	0.42	1.09	0.91	132	100.7	933.3	17.49	0.41	1.09	0.91
53	38.8	914.3	18.32	0.44	1.13	0.96	133	101.2	721.9	15.99	1.07	1.50	1.23
54	39.2	887.9	16.27	0.38	0.88	0.71	134	103.0	413.7	20.00	0.87	1.33	0.98
55	40.0	932.2	21.36	—	1.62	1.35	135	103.1	959.1	21.39	—	1.84	1.60
56	40.1	950.0	22.40	—	—	1.40	136	103.1	467.3	19.24	0.58	1.23	1.06
57	40.4	491.4	18.36	0.40	1.06	0.91	137	103.6	150.7	20.29	0.99	1.46	1.10
58	43.8	989.0	22.49	—	1.57	—	138	105.8	214.9	16.72	0.41	1.03	0.87
59	44.2	356.5	21.04	—	1.57	1.22	139	106.1	911.1	21.79	—	1.83	—
60	44.3	122.8	19.25	0.63	1.17	0.99	140	106.4	293.9	22.36	—	1.55	—
61	44.9	1014.1	21.89	—	1.81	—	141	106.7	245.3	22.11	—	1.13	1.24
62	45.9	568.6	15.86	1.37	1.55	1.23	142	106.9	268.5	19.78	0.78	1.34	1.12
63	46.1	817.5	22.05	—	1.79	1.80	143	107.0	540.7	17.93	0.80	1.20	0.97
64	47.2	631.8	19.61	0.75	1.29	1.08	144	109.3	372.6	18.20	0.46	1.13	0.98
65	47.8	717.7	20.34	1.17	1.45	1.14	145	109.6	428.6	22.17	—	1.64	1.34
66	49.7	79.8	17.66	0.50	1.06	0.88	146	110.6	437.2	21.68	—	1.69	1.51
67	50.2	66.0	17.91	0.41	1.09	0.92	147	111.6	692.8	22.08	—	1.21	1.02
68	50.2	349.7	22.15	—	1.70	1.79	148	112.8	509.1	22.19	—	1.97	1.55
69	50.3	137.1	18.52	0.71	1.33	1.14	149	113.1	984.8	21.31	—	1.44	1.28
70	51.4	553.4	18.88	0.61	1.23	1.00	150	113.4	409.7	19.89	0.91	1.38	1.19
71	51.8	378.2	19.15	-0.34	0.26	0.21	151	114.7	103.9	15.61	1.45	1.57	1.23
72	52.9	737.9	22.46	—	1.92	—	152	115.7	278.7	17.33	0.36	1.01	0.85
73	54.0	306.2	22.33	—	—	1.50	153	115.8	163.0	15.85	0.19	0.69	0.56
74	55.7	448.3	20.31	—	1.67	1.48	154	115.9	623.8	19.65	0.73	1.42	1.17
75	56.3	531.5	17.00	0.39	1.00	0.84	155	115.9	507.4	19.97	0.41	1.22	1.08
76	58.7	696.7	17.33	0.50	1.17	0.98	156	117.4	126.7	16.30	0.44	1.08	0.91
77	59.4	725.4	21.08	0.62	1.33	1.00	157	117.5	780.4	20.06	0.76	1.38	1.12
78	59.6	260.5	20.21	0.87	1.32	—	158	118.7	983.9	21.09	—	1.68	1.54
79	59.8	221.2	17.06	0.33	1.00	0.85	159	119.2	658.7	19.89	0.42	1.24	0.98
80	60.5	455.3	19.52	0.71	1.24	1.04	160	119.5	63.2	18.44	0.50	1.18	1.02

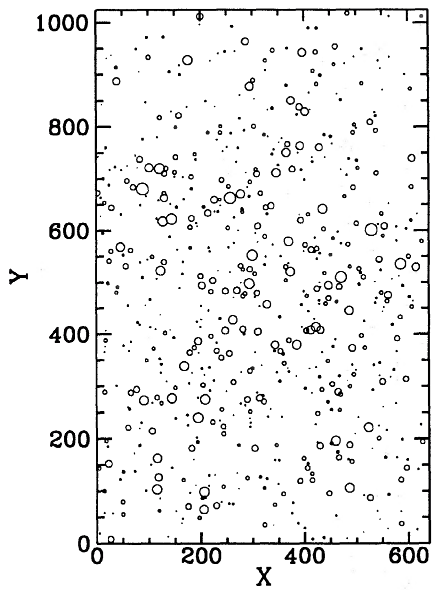

FIG. 2. Identification chart of NGC 7044. All the stars measured in V and at least, another band are shown. Circle sizes are proportional to the brightness in the V passband. The coordinates are CCD pixels and correspond to the X and Y values given in Table 2 made available through the ApJ-AJ CDROM series. North is left and East is bottom.

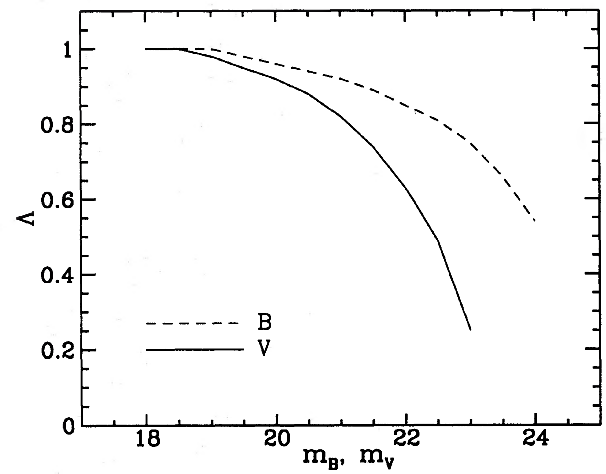

FIG. 3. Curves of completeness for B (dashed line) and V (solid line). The limiting magnitudes, defined as the magnitudes for which the completeness factor is 50%, are $B\simeq 24.1$ and $V\simeq 22.6$. The photometry is deeper in B, but this is caused by the red colors of the stars (see text for details).

stars, has been followed to estimate the photometric errors and the completeness of our data. This method has been discussed by several authors (see, for example, Stetson 1987), and is the best to estimate the actual errors of the photometry, and the completeness factor, both as a function of the magnitude. The analysis has been performed only in the B and V bands. A total of eight trials were carried out in each band, including 40 stars in each trial with magnitudes ranging from 19.6 to 23.6 in B and 18.9 to 22.9 in V. A summary of the results is given in Table 3, which lists the magnitude intervals (column 1); the total number of stars injected at each interval ($N_{\rm inj}$); the number of recovered stars ($N_{\rm rec}$); the corresponding factor of completeness Λ, obtained after fitting a curve to $N_{\rm rec}/N_{\rm inj}$ vs magnitude; the mean value ($\langle m_{i-r}\rangle$) of the distribution of $m^i_{\rm inj}-m^i_{\rm rec}$, where $m^i_{\rm inj}$ is the magnitude assigned to the injected artificial star i, and $m^i_{\rm rec}$ the magnitude recovered for it by ALLSTAR; and the square root of the quadratic mean of the values $m^i_{\rm inj}-m^i_{\rm rec}(\Sigma)$. This last figure can be assumed as representative of the actual error of the photometry at each magnitude interval.

Figure 3 shows the completeness curves in B and V, obtained after a fitting to the values listed in Table 3. The limiting magnitudes of our sample (defined as the magnitude at which we detect 50% of the stars) are about $B\simeq 24.1$ and $V\simeq 22.6$. On the other hand, small systematic departures between the injected magnitudes and the recovered ones ($\langle m_{i-r}\rangle$) are present. This kind of deviation affects mainly the faint end of the magnitude distribution, and is also produced by the completeness limit.

Once the Λ values have been obtained for B and V (we will refer to them as Λ_B and Λ_V), the correction of incompleteness of a given area in the CM diagram, say $V=m$ and $(B-V)=c$, can be done following different criteria. Here we employ the minimum between $\Lambda_V(m)$ and $\Lambda_B(m+c)$ to perform this correction. Our B photometry is deeper than the V one, but this is compensated by the fact that the stars of the lower main sequence (MS) of the cluster have $(B-V)$ about 1.0 to 1.5. In fact, all along the MS the Λ values of each pair $[\Lambda_V(m),\Lambda_B(m+c)]$ are very similar.

4. PHOTOMETRIC DIAGRAMS

Figures 4(a)–4(c) show the V vs $(U-B)$, V vs $(B-V)$, and the V vs $(V-R)$ CM diagrams, respectively.

TABLE 3. Errors and completeness factors in B and V.

Mag. bins	N_{inj}	N_{rec}	Λ	$<m_{i-r}>$	Σ
		1200 s B frame			
19.60–20.09	52	49	96	0.00	0.01
20.10–20.59	41	38	94	0.00	0.01
20.60–21.09	43	38	92	0.00	0.01
21.10–21.59	27	24	89	0.00	0.02
21.60–22.09	44	41	86	0.00	0.01
22.10–22.59	41	32	82	0.00	0.03
22.60–23.09	38	31	76	0.01	0.06
23.10–23.59	34	21	67	0.00	0.09
		800 s V frame			
18.90–19.39	28	27	98	0.00	0.01
19.40–19.89	41	38	95	0.01	0.02
19.90–20.39	41	29	91	0.01	0.02
20.40–20.89	42	37	87	0.01	0.03
20.90–21.39	48	40	81	0.01	0.04
21.40–21.89	43	30	72	0.03	0.11
21.90–22.39	40	23	60	0.03	0.11
22.40–22.89	37	17	46	0.04	0.17

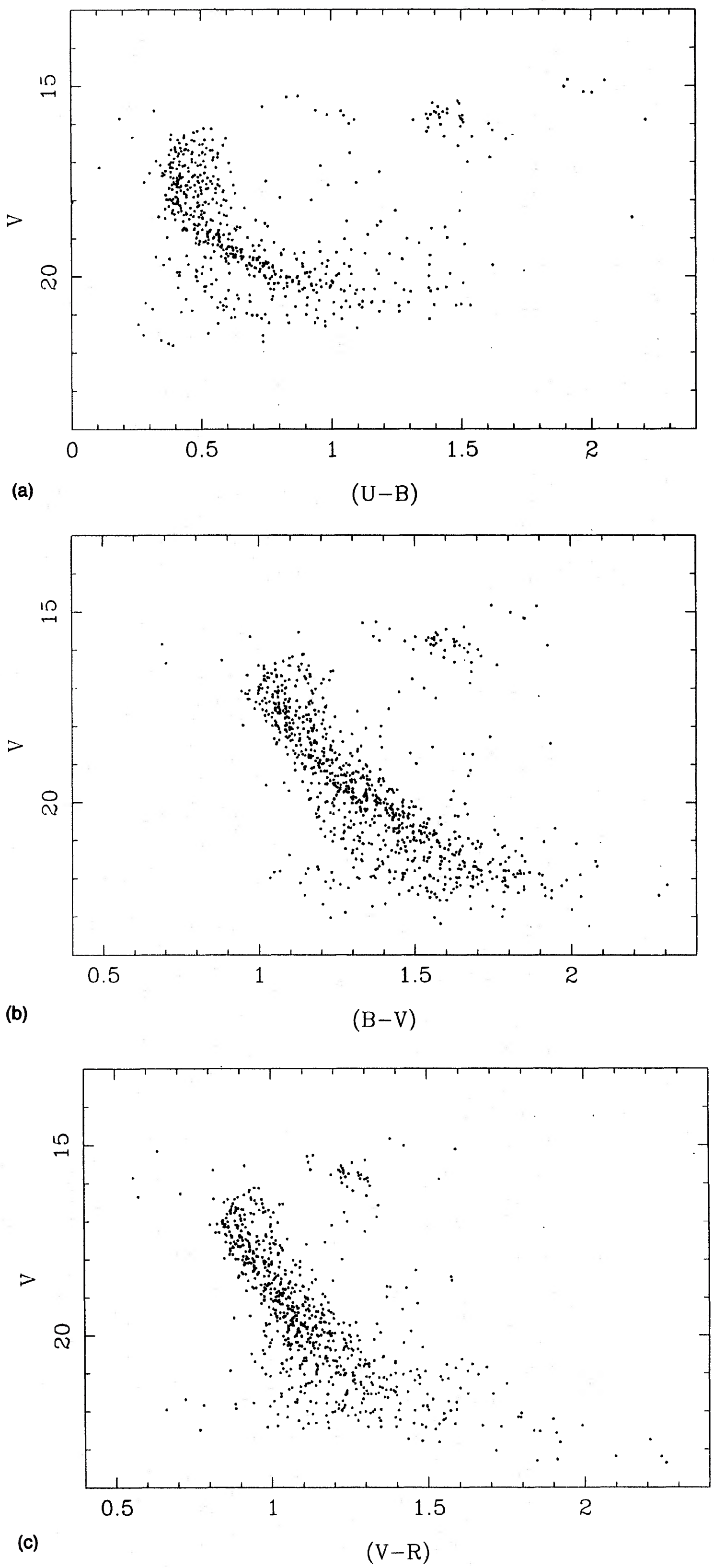

FIG. 4. (a)–(c). The V vs $(U-B)$, V vs $(B-V)$, and V vs $(V-R)$ CM diagrams for the stellar content of NGC 7044. Apparent magnitudes and colors are shown.

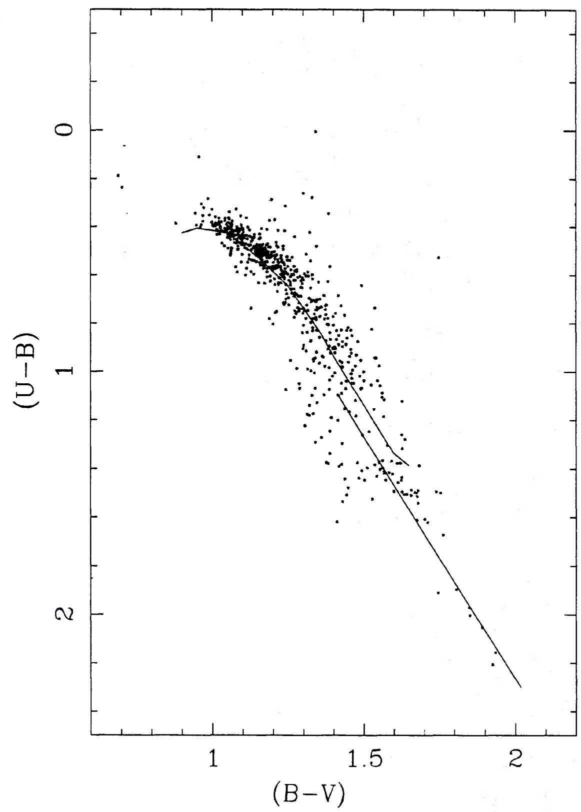

FIG. 4. (d) The two-color $(U-B)$ vs $(B-V)$ diagram for the stellar content of NGC 7044. The Hyades ZAMS and giant lines are also plotted for comparison, with color excesses and reddening slopes of 0.55–0.72, and 0.564–0.9, respectively.

The exposure time of the R frame (see Table 1) was too short, hence causing the completeness of the V vs $(V-R)$ diagram to be less than that of the V vs $(B-V)$ one. For this reason, the discussion of the main CM morphological features of this cluster will primarily be based on the observational V vs $(B-V)$ diagram. In any case, the locus of the MS is clearly visible in all three CM diagrams, with the top at about $V=16.2$. The upper part of the MS, around and above the estimated position for the turnoff, appears wider than other fainter sections, where a larger intrinsic dispersion has been estimated (see Table 3), suggesting that this broadening is not of a stochastic nature. This feature has been observed previously in other intermediate-age and old clusters, and its origin has been assigned to several causes: binarity, variable reddening, and noncoeval formation, among others.

The cluster does not show a well developed giant branch, but a rich red clump centered at about $V=15.9$, $(B-V)=1.60$, $(V-R)=1.25$. In the V vs $(U-B)$ CM diagram [Fig. 4(a)] these stars appear clearly split into three groups: the bluest, with $(U-B)$ spread between 0.7 and 1.1, and containing nine stars; the intermediate one, at $(U-B)$ between 1.3 and 1.7, with 32 stars; and the reddest, with five stars, at $(U-B)$ about 2.0, that delineates a sketch of asymptotic branch. Whether these stars are field stars or cluster members cannot be established with photometric information only. However, if as a first approximation we assume them as members, the bluest group can be interpreted as formed by binary stars of the composite (gK+dA) type (see Mermilliod & Mayor 1989 and, for synthetic simulations, Aparicio *et al.* 1990). On the basis of this interpretation, the ratio of the number of stars in the bluest group to the sum of stars in the reddest and in the intermediate groups, provides an estimate of 0.22 for the fraction of binaries in the cluster. This is likely to be a lower limit, because some of the stars in the intermediate and reddest groups themselves could also be binaries in which the secondary is too weak to produce detectable effects.

Finally, we note the presence of a small number of stars populating the lower right part of the CM diagrams. These objects are likely to be foreground stars and their small number suggests that the contamination by field stars is not very large, at least in the field covered by our observations. However, NGC 7044 is located in a rich area of the Milky Way, so any result based on star counts (like the former one about the binaries content) has to be considered with care, at least until more accurate information about the field stars becomes available.

The overall morphology of the three CM diagrams [Figs. 4(a)–4(c)] resembles that of the intermediate-age open clusters (B84), in which the turnoff mass, and the mass of the red giant stars, is large enough (above the critical mass m_c described in Sec. 1) to allow a mild He core ignition, so avoiding the formation of a developed giant branch. Instead, a clump populated by stars in the He core burning phase is formed, the so-called Red Giant Clump (RGC). In Sec. 6 we shall come back to the discussion of the RGC in NGC 7044.

The $(U-B)$ vs $(B-V)$ color–color (CC) diagram is shown in Fig. 4(d). The main group of stars in this diagram corresponds to the MS phase. No evidence of stars affected by large differential reddening is apparent in this plot, but there are some objects slightly shifted to the right of the mean locus. In addition to stars numbers 11 and 653 (see table of photometry (Table 2) in the ApJ-AJ CD ROM series), placed far to the right side of the main group, there are about 20 stars with, apparently, some positive differential reddening. They are spatially spread over the whole field, and located down and towards the left of the MS on the CM diagrams. In particular, they constitute 50% of the group of stars at V about 20 to 21 and $(U-B)$ about 0.4 to 0.7 that appear to deviate from the MS in the V vs $(U-B)$ CM diagram. The weakness of these objects leads us to suggest photometric errors as the main cause of this departure, however the comparison of their positions on the V vs $(B-V)$ and V vs $(U-B)$ CM diagrams seems to indicate that most behave as background stars.

5. PHYSICAL PARAMETERS

5.1. Reddening, Metallicity, and Distance Modulus

The $(U-B)$ vs $(B-V)$ diagram has been used to estimate the color excess and metallicity simultaneously. To do so, we use the location on the diagram of both the giants and unevolved main-sequence members of the cluster. The

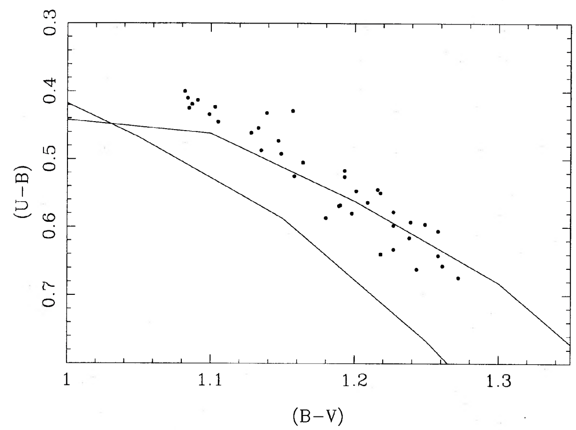

FIG. 5. Plot of the selected dwarf cluster members (see Sec. *5.1*) in the $(U-B)$ vs $(B-V)$ diagram. The Hyades ZAMS line, shifted for color excesses $E(B-V)=0.45$, and $E(B-V)=0.60$, is also plotted.

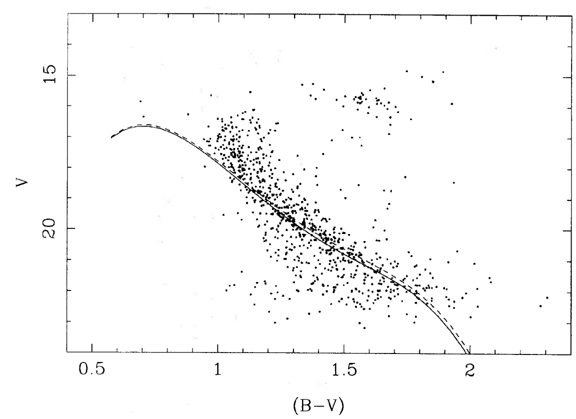

FIG. 6. The V vs $(B-V)$ color–magnitude diagram with the V89 solar ZAMS, shifted to account for $E(B-V)=0.57$ and $(m-M)_0=12.4$. The two lines shown are the result of using a constant absorption coefficient, $A_V/E(B-V)=0.72$ (dashed line), and the coefficients given in B78 (continuous line).

procedure requires the use of representative points of member stars only, avoiding also, as much as possible, the inclusion of binaries, and, particularly among the main-sequence objects, those which could have evolved above the ZAMS. In the absence of any spectroscopic information to ascertain the membership of individual stars, we must rely on the positions of representative points on the CM diagram. In this context, the combined use of the V vs $(B-V)$, V vs $(U-B)$, and V vs $(V-R)$ diagrams provides a useful tool to make a reliable discrimination of nonmembers.

To select the unevolved dwarf stars, we estimate a lower envelope of the main sequence in the V vs $(B-V)$ CM diagrams, between 18.0 and 20.0 in V [compare Fig. 4(b)]. Two lines parallel to this envelope, running 0.1 mag below and 0.2 mag above, then define a box which is considered to contain a reliable sample of unevolved dwarfs. Those stars deviating significantly from similar loci in the V vs $(U-B)$ and/or V vs $(V-R)$ diagrams, are rejected. In this way, we are left with a sample of 39 *bona fide* unevolved main-sequence cluster members. As giant members, we select in principle all the stars belonging simultaneously in the three diagrams to the conspicuous clump or the outline of asymptotic giant branch. This leads to a sample of 21 objects, which are considered as giant cluster members.

To estimate the reddening and metallicity simultaneously, we follow the approach by Twarog *et al.* (1993) in their exhaustive analysis of NGC 5822 (this paper is hereafter referred to as T93). We shift the ZAMS reference line in the two color $(U-B)$ vs $(B-V)$ diagram, for different values of the color excess, and compute the $\delta(U-B)$ values. After individual corrections with guillotine factors, interpolated in the values tabulated by Sandage (1969), a mean $\delta(U-B)_{0.6}$ is obtained $[(U-B)_{\rm line}-(U-B)_*$ at $(B-V)_0=0.6]$, which correlates with [Fe/H] (Carney 1979; Cameron 1985). Once the mean $\delta(U-B)_{0.6}$ is computed for a range of plausible reddening values, further constraints can be set by performing the same operation with the selected giants and the giants reference line. This requires that their mean $\delta(U-B)$ [actually $\delta(U-B)_{1.0}$] equals $\delta(U-B)_{0.6}$. In this procedure, we consider the color excess of the giants to be reduced by a factor 0.94 with respect to the dwarfs (Fernie 1963; Buser 1978, hereafter referred to as B78).

A critical point in performing this task is the choice of reference lines and reddening slopes. The semiempirical studies published in the literature, (Crawford & Mandwewala 1976; B78) result in derived slopes, which show appreciable differences in their values, as well as variations with spectral type, and/or with the region of the galaxy. Here we follow T93, adopting the procedure deviced by Hartwick & McClure (1972), and the Hyades ZAMS (Sandage & Eggen 1959) and giants line (Boyle & McClure 1975). They have the advantage of being fully empirical relations, both for dwarfs and giants in the same cluster. The assumption of equal $\delta(U-B)$ in both samples seems therefore well justified. Furthermore, the application of the guillotine factors is more sound when using the Hyades ZAMS, since they were computed using this line as a basis (Sandage 1969)

A first delimitation of the possible range of $E(B-V)$ values is established just by using the location of the selected sample of dwarf stars in the CC diagram. Figure 5 shows a plot of our selected dwarf sample in the CC diagram, with the Hyades ZAMS shifted for two extreme reddening values, 0.45 and 0.6. We appreciate that $\delta(U-B)$ is always larger than zero, indicating a metallicity lower than that of the Hyades. Furthermore, $E(B-V)$ has to be smaller than 0.6, since at this, and larger values, stars at $(B-V)_0 \geqslant 0.6$ would show no $\delta(U-B)$, or even negative values, otherwise smaller than the value for bluer stars. The giants line is now shifted with $E(B-V)$ values in this range, and the corresponding mean $\delta(U-B)$ is computed. The condition of an equal $\delta(U-B)$ for the ZAMS and the giants stars gives a formal solution at $E(B-V)=0.574$, $\delta(U-B)_{0.6}=0.025$. With Carney's (1979) linear relation, valid for [Fe/H] > −1, we obtain [Fe/H] = −0.009, which would increase to solar metallicity considering [Fe/H]=0.12 for the Hyades (T93), instead of 0.11, as assumed by Carney (1979).

The distance modulus can now be determined by means of the ZAMS fitting procedure. We apply here the semiempirical method designed by VandenBerg & Poll (1989; hereafter referred to as V89), to derive ZAMS for any values of metallicity and Helium contents, which have been found to produce solar ZAMS in excellent agreement with the relation of Sandage & Eggen (1959). To shift the line in the V vs $(B-V)$ plane we apply a constant absorption coefficient, $A_V/\mathrm{E}(B-V)=3.2$, and also the coefficients given in B78. Both lines are plotted in Fig. 6, which shows the best fit to our CM diagram for a true distance modulus, $(m-M)_0=12.4$, with an upper limit for the uncertainty of 0.1.

Before going on to the comparison of our observed CM diagram with theoretical isochrones, some comments have to be made, concerning the use of color-dependent reddening slopes. The works of Crawford & Mandwewala (1976) and B78 already quoted, show two main features which should be considered in this context: first, a clear variation of reddening slopes and absorption coefficients with spectral type, and second, higher values of these coefficients in the ranges of $(B-V)_0$ values covered by our samples of dwarfs and giants.

The variations are not negligible, mainly in the presence of high reddening, since they will produce significant deformations of the reference lines when shifted, as has been exemplified by Cameron (1985) for the ZAMS line. This can also be noticed by shifting the V89 ZAMS in the CM diagram with the absorption coefficients given by B78 for the stars of luminosity class V. The fit to the main sequence clearly improves, in that the slope is better reproduced, as opposed to the application of a constant value (compare the continuous and dashed lines in Fig. 6). This indicates that the fine variations of the absorption coefficients derived in B78 could be at work in the present case.

But the most conspicuous difference in the final estimates for reddening and metallicity arises from the differences in the values of the slopes themselves. Being much higher than the value of 0.72 used by Hartwick & McClure (1972), they would lead to higher $\delta(U-B)$, giving in turn a metallicity value significantly lower than the solar one. As an example, we have estimated the reddening and metallicity as explained at the beginning of this subsection, shifting now the Hyades ZAMS and giants line with the reddening slopes of B78. The main difference appears in the $\delta(U-B)$ values deduced for the dwarfs, leading to $\mathrm{E}(B-V)=0.41$, and $\delta(U-B)_{0.6}=0.23$. We note in passing, that just by including a second-order term in the reddening slope,

$$\mathrm{E}(U-B)/\mathrm{E}(B-V)=0.72+0.05\mathrm{E}(B-V),$$

gives $\mathrm{E}(B-V)=0.54$, and $\delta(U-B)_{0.6}=0.06$, which means a metallicity of [Fe/H] = −0.18.

The net effects of considering larger slopes are therefore lower color excess and metallicity values, leading further to a fainter ZAMS as designed by V89, and consequently a much smaller true distance modulus. Albeit self-consistent, these solutions would however lead to an excessively high age for the cluster, in contradiction with the morphology of the CM diagram, where the difference in V between the RGC and the turnoff is more indicative of an intermediate age, not exceeding, say, 3×10^9 yr. The possibility of interpreting the most luminous turnoff stars as binaries, would allow a higher age limit, but it would not reach the age value implied by the too small distance in luminosity between the turnoff and the RGC.

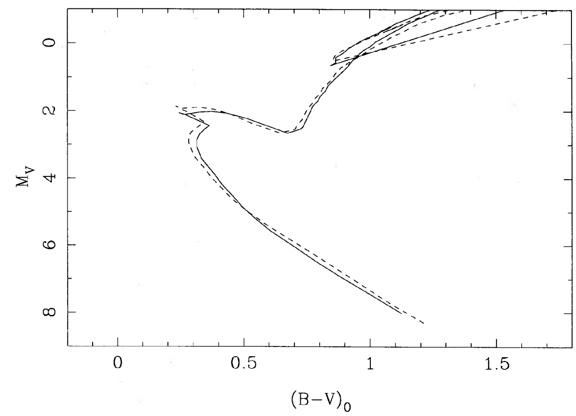

FIG. 7. Comparison between the isochrone of A93 for $Y=0.25$, $Z=0.008$ (continuous line), with that for $Y=0.28$, $Z=0.020$, shifted to account for a corresponding metallicity of [Fe/H] = −0.408 (dashed line). Both isochrones have been previously corrected for the He contents difference to the one assumed as solar, $Y=0.27$. All shifts are computed with formulae 6 to 9 (see text).

We note finally that the uncertainties present in our U photometry should sensibly affect the precision of our metallicity estimates. In fact, the dispersion of the mean $\delta(U-B)$ in our dwarfs sample amounts to 0.02, which leads to an uncertainty of 2 dex in the metallicity estimate. Moreover, all these values are affected by the zero-point error of our photometry, that is about 0.02 to 0.03 for all color indices, and for V (see Sec. 2). Taking this into account, we definitely adopt the following set of parameters:

$$\mathrm{E}(B-V)=0.57\pm0.03,\quad [\mathrm{Fe/H}]=0.0\pm0.2,$$

$$(m-M)_0=12.4\pm0.1 \tag{5}$$

with the precaution of considering the metallicity estimate as an upper limit. Assuming a solar radius $R_\odot=8.5$ Kpc, the cluster is then located at a galactocentric radius $R_G=9$ Kpc.

5.2. *The age of NGC 7044*

In this subsection our aim is to estimate the age of the cluster by comparing the CM diagram with theoretical isochrones, computed with and without considering convective-core overshooting during the phases of nuclear

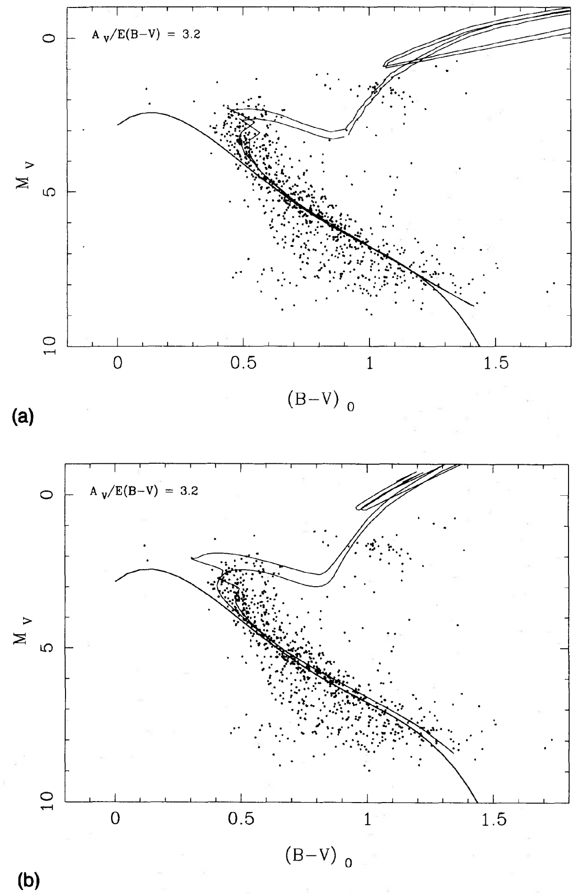

FIG. 8. Absolute magnitude vs intrinsic $(B-V)_0$ diagram. (a) A93 isochrones for log age(y) = 9.4, and 9.5. (b) C92 isochrones for log age(y) = 9.3, and 9.5. Both isochrones are plotted, after correcting for composition and solar colors as explained in the text. The stars have been dereddened with a constant value for the absorption, A_V/E$(B-V)$ = 0.72.

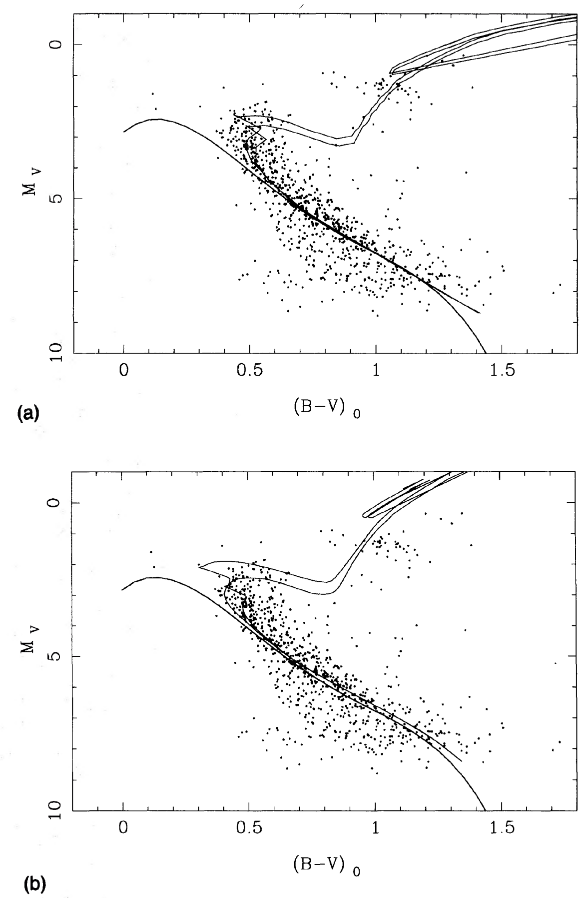

FIG. 9. (a) and (b) The same as Fig. 8 with the stars dereddened by means of the absorption coefficients given in B78. An improved fit can be appreciated, as opposed to that shown in Fig. 8.

burning. The better or worse quality of the fitting to the different models will help us to adopt final estimates for the photometric parameters, and also provides clues to decide whether the overshooting approach should be preferred. The most recent works in this field are those published by Alongi *et al.* (1993) (models with overshooting) and Castellani *et al.* (1992) (models without overshooting), hereafter referred to as A93 and C92, respectively. Before carrying out the comparison, we apply to both sets of isochrones a kind of renormalization procedure, designed and explained in detail by T93. It consists in computing the required shifts in magnitude and color to be applied to every isochrone, in order to bring them first to a helium content of 0.27, considered as solar by V89, whose ZAMS was used to estimate the distance modulus. Once isochrones of the same solar abundance are obtained in both sets, new shifts are applied to make the model of $1\mathscr{M}_\odot$ to have M_V=4.84 and $(B-V)_0$=0.65, at an age of 4.6×10^9 yr. They amount to $\Delta M_V=-0.134$, $\Delta(B-V)=0.045$ for the A93 isochrones, and $\Delta M_V=-0.27$, $\Delta(B-V)=0.0$ for the C92 ones. Final shifts in magnitude and color are applied to obtain isochrones for the precise metallicity value desired. The shifts to correct for helium contents and metallicity differences are both computed with interpolation in Table 3 of V89, completed with the results of VandenBerg & Bridges (1984) for lower metallicities. The resulting formulae for ΔM_V and $\Delta(B-V)_0$ are

$$\Delta M_V(Y)=-2.261+8.360Y, \tag{6}$$

$$\Delta(B-V)(Y)=-0.486+1.880Y, \tag{7}$$

$$\Delta M_V([\mathrm{Fe/H}])=0.008+1.530[\mathrm{Fe/H}] +0.514[\mathrm{Fe/H}]^2, \tag{8}$$

$$\Delta(B-V)([\mathrm{Fe/H}])=-0.007+0.512[\mathrm{Fe/H}] +0.315[\mathrm{Fe/H}]^2. \tag{9}$$

The method yields satisfactory results, as can be seen from Fig. 7, where an isochrone of A93 for Y=0.25, Z=0.008 (continous line) is shifted to account for a Y difference of 0.25 to 0.27, and compared with that computed with Y=0.28, Z=0.020, and corrected for helium contents (0.28 to 0.27), and metallicity (0.0 to −0.4). As can be seen in the figure, the magnitude differences in the main sequences, of about 0.1 mag, are below the uncertainty of the distance modulus determination by means of the

ZAMS fitting, and the shifted isochrone reproduces very closely the position of the giant clump as predicted by the one actually computed, both in color and in magnitude.

The comparison of our CM diagram with the isochrones can be now performed after shifting the stars in V and $(B-V)$, assuming $A_V/E(B-V)=3.2$ in the whole spectral type range. Figures 8(a) and 8(b) show, respectively, the A93 and C92 isochrones which best fit the data. The ZAMS of V89 for solar metallicity are also plotted. Two remarks are called for here: first, as noted in the foregoing subsection, the fit of the main-sequence slope seems somewhat defective, for both isochrones and ZAMS; second, the observed absolute magnitude of the RGC differs by more than 1 mag with that predicted by the models. We recall again the improvement that can be achieved by considering variations of the absorption coefficient with spectral type, and in particular a higher value for the giants than that for the ZAMS. In Fig. 9(a) and 9(b), we have plotted the same isochrones as in Fig. 8, now using the absorption coefficients given in B78 to deredden the stars. The general improvement in the quality of the fitting is clearly seen when comparing these plots with those in Fig. 8. The discussion of the clump properties, in Sec. 6, will be based on these latter fits.

Second, independently of the values used for the absorption coefficients, we observe a better general agreement between models and observations, when the overshooting isochrones are used. The most prominent difference with respect to the nonovershooting models, appears in the quality of the reproduction for the absolute magnitude of the RGC. As noted by T93, this fact is determined by the inability of the nonovershooting C92 isochrones to predict the increasing absolute magnitude of the clump with increasing age.

Finally, we note that both models lead to an age estimate around log age$(y)=9.4$. However, we point out that the overshooting isochrones would give a slightly lower age than those computed without overshooting, while exactly the opposite should be expected.

6. THE RED GIANT CLUMP

The location of the RGC in the color–magnitude diagram of NGC 7044 deserves some further comment. In a previuously published analysis of this cluster (Kalużny 1989) the RGC is assumed to be located at $[M_V,(B-V)_0]=(0.6,0.94)$, on the basis of similarities between the CM diagram of the cluster and those of NGC 7789 and Praesepe. However, in the statistical analysis by B84, NGC 7789 turns out to show a peculiar absence of faint red stars—in this sense being far from a typical example of intermediate age open cluster—and Praesepe is one of the youngest in the sample, judging from its relatively blue color at the turnoff. Deriving photometric parameters of NGC 7044 from a comparison with these sources might therefore be misleading.

On the other hand, the results of our analysis indeed show the clump of NGC 7044 to be located at a somewhat lower luminosity and redder color than most of the clusters in the intermediate age subsample of B84. Their Fig. 3 is quite clarifying in this context. It represents the magnitude of the faintest red giant versus the intrinsic color of the turnoff, for a large sample of intermediate age and old open clusters. Using their terminology, for NGC 7044 we take the values from our photometry, $(B-V)_{0,t}=0.42$, and $M_{b,\mathrm{RG}}=1.5$ as the faintest magnitude in the clump [see, for instance, Fig. 9(a)]. These values place the representative point of our cluster on the old side of the separation line between the intermediate-age and old subsamples of B84. With the solution adopted here, NGC 7044 turns out to be very similar to NGC 752 in many of its features, as listed in the compilation of B84. It actually shows a slightly redder color at the turnoff, which should reflect the derived higher metallicity, [Fe/H]=0.00, as compared with the recent determination of [Fe/H]=−0.09 for NGC 752 (Hobbs & Thorburn 1992).

A recent photometric analysis of NGC 752 (Dzérvitís & Paupers 1993), shows its RGC as composed of two subgroups at different luminosity, which they suggest as representing the two different evolutionary states of core helium burning, and early ascent of the red giant branch (EAGB). The presence of binaries, however, as mentioned in Sec. 4, and the possible contamination of field stars

TABLE 4. Star counts for different spatial sections and different M_{V_0} vs $(B-V)_0$ areas of NGC 7044.

Section	N_R	N_{MS_u}	N_{MS_d}	$N_R/(')^2$	$N_{MS_u}/(')^2$	$N_{MS_d}/(')^2$
Whole	43	199	306.7	3.7	17.3	26.6
$r<150$	9	29	42.2	7.1	22.8	33.2
$150\leq r<225$	11	38	44.4	7.0	24.1	28.1
$225\leq r<300$	11	49	82.2	5.0	22.1	37.0
$300\leq r<375$	6	38	55.6	2.7	16.9	24.7
$375\leq r$	6	45	82.2	1.4	10.7	19.6

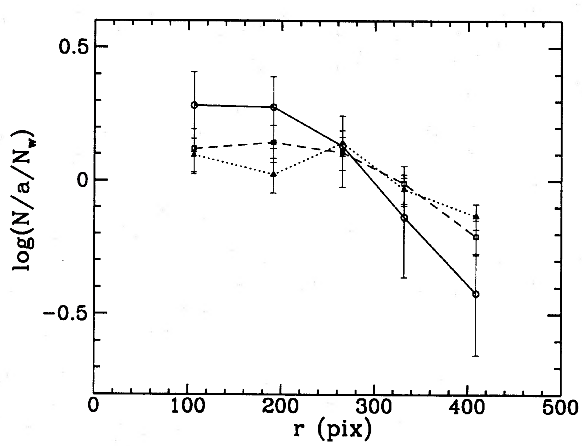

FIG. 10. Logarithm of the relative number of stars (normalized to the area and to the total number of stars of the corresponding class in the whole frame) in the three zones of the CM diagram, as a function of the distance from the barycenter of the cluster. Full line plus circles correspond to the red giants; dashed line plus squares correspond to the MS stars with $2.5\leqslant M_{V_0}<4.5$ and dotted line plus triangles correspond to MS stars with $4.5\leqslant M_{V_0}<6.5$ (see text for details).

TABLE 5. The luminosity and mass functions of NGC 7044.

M_V	log m	N_C	$\xi(\log m)$
2.0–2.5	0.27 – 0.215	37.0	2.83
2.5–3.0	0.215– 0.16	39.0	2.85
3.0–3.5	0.16 – 0.115	61.0	3.13
3.5–4.0	0.115– 0.07	54.5	3.08
4.0–4.5	0.07 – 0.03	56.7	3.15
4.5–5.0	0.03 – –0.01	63.2	3.20
5.0–5.5	–0.01 – –0.045	87.0	3.40
5.5–6.0	–0.045– –0.08	98.8	3.45
6.0–6.5	–0.08 – –0.11	83.7	3.45
6.5–7.0	–0.11 – –0.14	93.8	3.50
7.0–7.5	–0.14 – –0.175	94.5	3.43
7.5–8.0	–0.175– –0.21	124.2	3.55

should be considered here. Going back to our CM diagrams [Figs. 4(a)–4(c)], we can detect in all them the presence of some red stars located below the clump, which could be considered as representative of the EAGB phase. This is however rather uncertain, in view of the field stars contamination of the diagrams. On the other hand, even if some of these stars were adscribed to the EAGB phase, this would imply a too low ratio of stars in this evolutionary state, with respect to the number of core He burning stars.

Assuming therefore that no visible signs of the EAGB phase are currently in our CM diagram, we may propose a further argument in favor of considering the presence of overshooting in the evolutionary computations. Independently of the quality of the fitting to the isochrones, shown in Figs. 8 and 9, we can look at the masses predicted by the different models for the stars at the He core burning stage. The C92 and A93 isochrones for log age 9.5 and 9.4, predict masses of $1.51\mathscr{M}_\odot$, and $1.44\mathscr{M}_\odot$ at this stage. In both cases, these values are below the predicted critical masses, separating the regimes of He flash and quiet onset of He burning. The discrepancy between predictions of the models, and the observed absence of delayed evolution in the first ascent of the giant branch in the cluster, would not only give support to the overshooting approach. It further suggests the need of considering a higher efficiency of convective-core overshooting in the evolutionary computations, particularly for the mass range considered in this context.

Summing up the discussion in this section, we consider our results for NGC 7044 to support the overshooting models. However, more abundant and precise information about membership of particular stars is needed before a conclusive analysis of this issue can be performed.

7. A BRIEF DISCUSSION ON THE SPATIAL DISTRIBUTION OF STARS IN NGC 7044

To analyze the differences of the stars populating different sections of the cluster, and following the criterion of Alfaro *et al.* (1992), we have subdivided the whole frame in five concentric circles of radii 150, 225, 300, 375, and $r > 375$, centered on the barycenter of the spatial distribution of stars, located at $x = 310$, $y = 498$ in pixel units. It is an interesting test to compare the relative number of stars

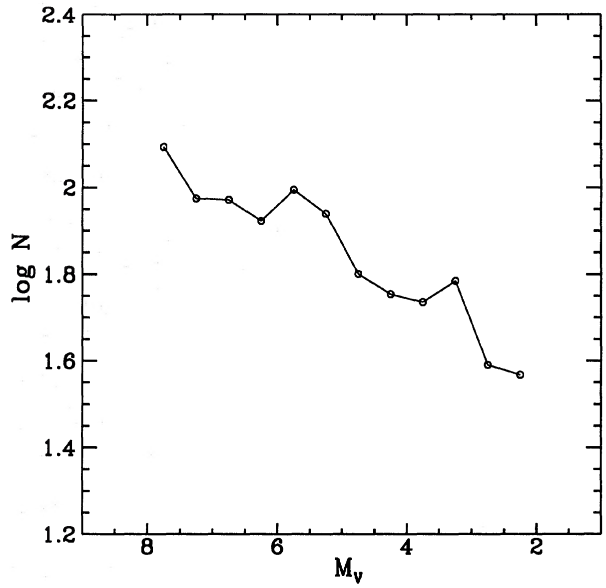

FIG. 11. The luminosity function of the MS stars of NGC 7044.

in different parts of the CM diagram for each section. Let us define three areas in the CM diagram: the red giant stars, the MS stars with $2.5 \leqslant M_V < 4.5$ and the MS stars with $4.5 \leqslant M_V < 6.5$. Following the theoretical data by A93 and using a Salpeter Initial Mass Function (IMF) (Salpeter 1955) to interpolate, the first group can be represented by a star with $1.46\mathscr{M}_\odot$, the second by a star with $1.24\mathscr{M}_\odot$, and the third by a star with $0.93\mathscr{M}_\odot$. The resulting numbers of stars in each group and for each annulus, including the results for the whole frame, are listed in Table 4. Columns 2 to 4 give the absolute numbers, divided by 0.9 in the case of stars with $4.5 \leqslant M_V < 6.5$ to correct for incompleteness. Columns 5 to 7 give the same values normalized to the area, in square arcminutes, of the corresponding section. The logarithm of the numbers listed in these columns, normalized to those of the whole frame for each class of stars, are plotted in Fig. 10, where the solid line corresponds to the red giants; the dashed line, to the MS stars with $2.5 \leqslant M_V < 4.5$; and the dotted line to MS stars with $4.5 \leqslant M_V < 6.5$. The error bars have been computed assuming a Poissonian statistic. The three distributions are inside the band defined by the error bars, but the distribution of the red stars ($1.46\mathscr{M}_\odot$) could be marginally decoupled from the distributions of both groups of MS stars (1.24 and $0.93\mathscr{M}_\odot$) in the sense that the stars turn out to be more massive the more concentrated to the center of the cluster. This could be accounted for by segregation of low mass stars, but in any case, the distributions of stars can be affected by field stars contamination. In particular, the minimum of the distribution of the less massive stars is probably a consequence of that contamination, that should affect the lower part of the main sequence and the outer regions of the cluster more strongly, since the number of member stars decreases.

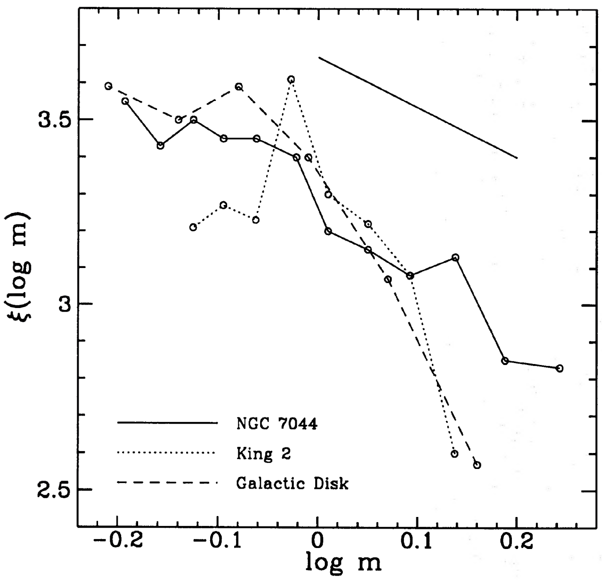

FIG. 12. The mass function of the stars of NGC 7044 compared to that of King 2 and the galactic disk. The straight line shows the Salpeter initial mass function with a slope $x=-1.35$. In the case of NGC 7044 and King 2, ξ is initial mass function of the the number of stars per unit of log m. In the case of the galactic disk, the number of stars is normalized to the area projected on the galactic plane, in pc^2. An arbitrary constant of 2 has also been added to the resulting logarithm.

8. THE LUMINOSITY AND MASS FUNCTIONS OF NGC 7044

Studies of LFs in intermediate-age and old open clusters set important constraints to the theories of star formation and supply new insights about the role played by the cluster dynamics on the actual luminosity distribution of evolved stars (Miller & Scalo 1979; Francic 1989). Table 5 summarizes the results obtained for the luminosity function (LF) and the mass function (MF) of the MS stars of NGC 7044, after correcting for incompleteness (see Table 3). Again, contamination by foreground stars could affect the results. In order to minimize its effects, the low luminosity red and blue stars [see Figs. 4(a) and 4(b) and the discussion in Sec. 4] have not been considered. In Table 5, column 1 lists the interval in M_V; column 2 gives the corresponding interval in logarithm of mass. The M_V—log m transformation has been made using the data from Table IV of Scalo (1986). Column 3 gives the number (N_C) of main-sequence stars inside each magnitude interval, after correcting for incompleteness using the data listed in Table 3. Finally, column 4 gives the logarithm of N_C normalized to the corresponding $\log m$ interval [$\log \xi(\log m)$]. Note that the small number of stars below $M_V=2.5$ simply reflects the rarefaction of stars at the turnoff, and that this part of the LF and MF is very sensitive to the amount of binary stars. Excluding this bin, we have fitted a power law of the classical type [$\xi(\log m)=Am^x$), obtaining $x=-1.66\pm0.06$, the Salpeter (1955) value being $x=-1.35$. The resulting LF (corrected for incompleteness) is shown in Fig. 11.

The question of whether the IMF is universal or whether would be affected by spatial or temporal variations is a classical one. Star clusters give a good opportunity to analyze these possible variations, and the differences from cluster to cluster inside our galaxy. However, an important limitation to this analysis is the mass segregation that might in principle affect most of the clusters. This effect produces a loss of low mass stars, modifying the shape of the MF of the cluster with time, in such a way that the actual IMF is difficult to recover. In our particular case, we are certainly not covering the whole area of the cluster in the secured frames, probably causing the loss of many low mass stars, and therefore biasing the estimates of the luminosity and mass functions to higher masses. In this sense, the value formerly quoted for the slope of the MF must be considered as an upper limit for that of the IMF. Moreover, the amount of binary stars as well as the field stars would also produce some effects on the slope of the MF (see Aparicio *et al.* 1990, for a detailed discussion of this aspect). In any case, a comparison between the MF of clusters and that of the galactic disk provides useful information for the general analysis of the IMF. In Fig. 12, the MF of NGC 7044 and King 2 (Aparicio *et al.* 1990) are shown together with the IMF of the disk of our galaxy (Scalo 1986). The range of masses covered by the MS stars of these clusters is especially important, because it includes the region of the inflexion observed in the IMF of the galactic disk. In the case of King 2, a similar inflexion is clearly appreciated, but it is not so clear in the MF of NGC 7044. However, nothing can be stated definitively in the present context, until more complete and better quality data are available for a larger sample of clusters.

9. SUMMARY AND CONCLUSIONS

The main results of our study can be summarized as follows:

(1) The CCD photometry in the Johnson–Cousins *UBVR* system has been secured for 896 stars in the field of the intermediate age open cluster NGC 7044. Color–magnitude diagrams, reaching 21 mag in $(U-B)$, and lower than 22 mag in $(B-V)$ and $(V-R)$ have been obtained. The significant width of the upper main sequence, near the turnoff, indicates the presence of a large content of binary stars. A rough estimate, based on the distribution of red evolved stars in all three CM diagrams, allows a guess of 0.22 for the fraction of binary members.

(2) The results of the photometric analysis are very dependent on whether, and to what extent, variations of reddening slopes and absorption coefficients with spectral type are considered to shift the reference lines in the photometric diagrams. The adopted values, after global consideration of the quality of the fitting with theoretical isocrones, are $E(B-V)=0.57\pm0.03$, $[\mathrm{Fe/H}]=0.0\pm0.2$, $(m-M)_0=12.4\pm0.1$. This metallicity is to be envisaged as upper limit to the actual value for the cluster.

(3) In the context of the adopted photometric solution, the age derived after comparing with model isochrones, with and without including convective core overshooting,

is constrained between log age(y) = 9.4, and log age(y) = 9.5. NGC 7044 turns out to show very similar features as the well known intermediate-age cluster NGC 752.

(4) The general agreement between observed and predicted features of the color–magnitude diagram favors the overshooting models versus the classical ones. In particular, the former better reproduce the observed location of the RGC, both in luminosity and color. In this context, the aspect of the RGC, showing no clear indications of stars in the EAGB phase, could be interpreted as an indication that efficiency of overshooting for stars around and below $1.5\mathscr{M}_{\odot}$ is larger than that considered in the models of A93.

(5) The luminosity and mass functions of NGC 7044 have been obtained. A classical power law has been fitted to the MF, obtaining a slope of $x = -1.66 \pm 0.06$ (Salpeter's value $x = -1.35$). The inflexion in the general IMF of the galactic disk at about 0.8 to $1\mathscr{M}_{\odot}$ is not visible in the MF of NGC 7044, but good quality data of more clusters are necessary to clarify this question. Finally, an analysis of the spatial distribution of stars suggests that a mass segregation mechanism is operating in the cluster.

This work was supported financially by the Instituto de Astrofísica de Canarias, the Research and Education Council of the Autonomous Government of Andalucía (Spain), and the Spanish Directorate General for Scientific and Technical Investigation (DGICYT), through Grant No. PB91-053. The observations were taken at the German–Spanish Observatory of Calar Alto (Spain). An anonymous referee is acknowledged for comments and suggestions, which greatly improved the final version of the paper.

REFERENCES

Alfaro E. J., Aparicio A., Delgado A., García-Pelayo, J. M., & Cabrera-Caño, J. 1992, AJ, 103, 204

Alongi, M., Bertelli, G., Bressan, A., Chiosi, C., Fagotto, F., Greggio, L., & Nasi, E. 1993, A&AS, 97, 851 (A93)

Aparicio, A., Bertelli, G., Chiosi, C., & García-Pelayo, J. M. 1990, A&A, 240, 262

Barbaro, G., & Pigatto, L. 1984, A&A, 136, 355 (B84)

Bertelli, G., Bressan, A., & Chiosi, C. 1985, A&A, 150, 33

Boesgaard, A. M., & Friel, E. D. 1990, ApJ, 351, 467

Boyle, R. J., & McClure, R. D. 1975, PASP, 87, 12

Buser, R. 1978, A&A, 62, 411 (B78)

Cameron, L. M. 1985, A&A, 146, 59

Carney, B. W. 1979, ApJ, 233, 211

Castellani, V., Chieffi A., & Straniero, O. 1992, ApJS, 78, 517 (C92)

Chiosi, C., Bertelli, G., Meyland, G., & Ortolani, S. 1989, A&AS, 78, 89

Crawford, D. L., & Mandwewala, N. 1976, PASP, 88, 917

Dzérvitís, U., & Paupers, O. 1993, ApSS, 199, 77

Fernie, J. D. 1963, AJ, 68, 780

Francic, S. P. 1989, AJ, 98, 888

Friel, E. D., & Janes, K. A. 1993, A&A (in press)

Geisler, D. 1987, AJ, 94, 84

Geisler, D., Claria, J., & Minniti, D. 1992, AJ, 104, 1892

Gilmore, G. 1990, in The Milky Way as a Galaxy, edited by R. Buser and I. King (University Science Books, Mill Valley, CA)

Hartwick, F. D. A., & McClure, R. D. 1972, PASP, 84, 288

Hobbs, L. M., & Thorburn, J. A. 1992, AJ, 104, 669

Janes, K. A. 1988, in Calibration of Stellar Ages, edited by A. G. D. Philip (Davis, Schenectady)

Kałużny, J. 1989, AcA, 39, 13

Landolt, A. U. 1983, AJ, 88, 439

Mateo, M., & Hodge, P. 1986, ApJS, 60, 893

Mazzei, P., & Pigatto, L. 1988, A&A, 193, 148

Mermilliod, J. C., & Mayor, M. 1989, A&A, 219, 125

Miller, G. E., & Scalo, J. M. 1979, ApJS, 41, 513

Neckel, Th., & Chini, R. 1980, A&AS, 39, 41

Salpeter, E. E. 1955, ApJ, 121, 161

Sandage, A. 1969, ApJ, 158, 115

Sandage, A. 1988, in Calibration of Stellar Ages, edited by A. G. D. Philip (Davis, Schenectady)

Sandage, A., & Eggen, O. J. 1959, MNRAS, 119, 278

Scalo, J. M. 1986, Fund. of Cosmic Physics, 11, 1

Stetson, P. B. 1987, PASP, 99, 191

Twarog, B. A., Anthony-Twarog, B. J., & McClure, R. D. 1993, AJ (in press) (T93)

Vallenari, A., Chiosi, C., Bertelli, G., Meylan, G., & Ortolani, S. 1993, AJ (in press)

VandenBerg, D. A., & Bridges, T. J. 1984, ApJ, 278, 679

VandenBerg, D. A., & Poll, H. E. 1989, AJ, 98, 1451 (V89)